Spectral Features Selection and Classification for Bimodal Optical Spectroscopy Applied to Bladder Cancer *in vivo* Diagnosis

Emilie Péry*, Walter C.P.M. Blondel*, Samy Tindel*, Maha Ghribi, Agnès Leroux and François Guillemin

Abstract—This paper describes an experimental study combining spatially resolved AutoFluorescence (AF) and Diffuse Reflectance (DR) fibred spectroscopies to discriminate *in vivo* between healthy and pathological tissues in a preclinical model of bladder cancer. Then, a detailed step-by-step analysis scheme is presented for the extraction and the selection of discriminative spectral features (correlation, Linear Discriminant and Logistic Regression Analysis), and for the spectroscopic data final classification algorithms (Regularized Discriminant Analysis and Support Vector Machines). Significant differences between healthy, inflammatory and tumoral tissues were obtained by selecting a reasonable number of discriminant spectral features from AF, DR and Intrinsic Fluorescence spectra, leading to improved sensitivity (87%) and specificity (77%) compared to monomodality (AF or DR alone).

Index Terms—autofluorescence, diffuse reflectance, bladder cancer, feature selection, supervised classification

ACRONYMS

AF	AutoFluorescence
a.u.	Arbitrary Units
CEFS	Collecting to Exciting Fiber Separation
CIS	Carcinoma *In Situ*
DR	Diffuse Reflectance
LDA	Linear Discriminant Analysis
LOO	Leave-One-Out
NADH	Nicotinamide Adenine Dinucleotide
(N)UV	(Near) Ultra-Violet
RDA	Regularized Discriminant Analysis
SD	Standard Deviation
Se, Sp	Sensitivity, Specificity
SVM	Support Vector Machines

I. INTRODUCTION

MORE than 85% of cancers arise inside the tissue upper layers (or epithelium) of the human body organs, among which 50% in hollow organs (aerial, digestive, urinary and genital tracts) [1], [2]. The detection of cancerous tissular lesions at their early stages of development is at stake in increasing the chances for health recovery with help of less aggressive treatments and reduced costs. Bladder cancer is the 7th most spread cancer in the world [3]. One of the main problems concerning bladder tumors is their high recurrence potential, especially in case of progression. Recurrence, with an important progression risk is often associated to Carcinoma *In Situ* (CIS) with multifocal and diffuse locations over the bladder internal wall.

Cystoscopy is the reference clinical examination allowing the physician to analyze visually the macroscopic aspect of the bladder surface and to locate suspicious or identified pathological lesions [4] [5]. Surgical biopsy followed by histopathological analysis is performed on the latter in order to identify and diagnose the exact nature and status of the tissue. Even without significant abnormalities, a number of biopsies is to be done, more or less randomly, or by following a systematic "grid-protocol". But the total number of biopsies on the overall surface is of course limited and this traumatic procedure has therefore a poor clinical sensitivity [6]. Furthermore, due to intrinsic characteristics (flat, non-papillary tumors, located at the mucous membrane), CIS may not be detected by conventional cystoscopy and recurrence risk is therefore increased.

In order to improve the efficiency of diagnostic procedures (like biopsy guiding), the efficiency of surgical treatments (lesion targeting and spatial outlining) and the one of individual patient follow-up, non invasive fibered optical spectroscopy methods are developed and applied to identify and characterize healthy and pathological tissue status *in vivo*. During the carcinogenic process, pathological tissues differentiate from healthy ones throughout a number of anatomical, biochemical and physiological modifications at the cellular and tissular levels with namely [7]–[11]: changes in the tissue structural organization (higher cell proliferation, epithelium thickening, infiltration in the surrounding tissues, neo-vascularization, cell disorientation), hyperchromatism (thickening and densification of chromatin), hyper-metabolism of the tumoral cells (increased production of NADH), increase of the cell nucleus

size, modifications of the interactions between cells... These physico-chemical, morphological, structural and functional modifications lead to changes in the optical properties of absorption and diffusion of light in the tissues, that can be detected at the early stages of hyperplastic (or cell abnormal proliferation) development.

Tissue optical spectroscopy for *in vivo* diagnosis (also sometimes called optical biopsy) consists in bringing a fiber optics probe at the contact with the tissue and in measuring the intensity spectra backscattered by the tissue under specific light excitation. Being fibered, the method can be applied through the operating channel of standard cystoscopes. The tissular volume in which the light propagates depends on the geometry of the probe, on the type of excitation and on the wavelength band of interest. In the UV-Visible wavelength range (typically 350-750 nm), these techniques are well adapted to the characterization of biological tissues of limited thicknesses such as bladder mucosa and the detection of epithelial or sub-epithelial lesions. The principle of spatially resolved spectroscopy (AutoFluorescence AF or Diffuse Reflectance DR) is based on the use of a multiple fiber probe with several CEFS (Collecting to Exciting Fiber Separation) to probe different tissue depths. In this way, tissue modifications due to pathology and located at various depths can be probed. Three main phenomena of light-tissue interaction can be more specifically exploited in the UV-Visible range of interest [12], [13]. Elastic scattering (due to changes of the refractive indices in the medium) is the major phenomenon in terms of light intensity magnitude and light-tissue interaction event probability. It allows the light to travel inside the tissue in all directions and to be partially back-collected at different points at the surface of the tissue after multiple scattering. The second one is a non-radiative process due to absorption by intrinsic chromophores (haemoglobin, melanin, water) i.e. without photon re-emission. The third process is due to the absorption by intrinsic fluorophores (collagen, elastin, NADH, flavins, porphyrins, etc.) followed by a radiative emission of fluorescence new photons.

The AF intensity spectra emitted by a biological tissue carries information linked to the biochemical nature and metabolic activity of the latter [14]. Exploiting and interpreting the results of AF measurements requires statistical and empirical analysis of the AF intensity spectra, because their spectral features are modified by the cross-contribution of absorption and diffusion that limits the extraction of quantitative biochemical data [15]. In order to exploit the complementary information linked to the localization and concentration of various intrinsic fluorophores, a few research teams have developed spectroscopic systems of multiple autofluorescence excitations applied namely to cervix, bladder and skin [16]–[19]. In the case of cancer diagnosis and tissue classification, optimal combinations of excitation wavelengths improving the classification performances are investigated. The few AF spectroscopy studies on human bladder cancerous lesion detection indicate that highest sensitivity and specificity values are obtained when low-UVA excitation wavelengths (below 340 nm) are used [20]. The main drawbacks of using these excitation low wavelengths are mutagenic risks for the irradiated tissues

and the need of specific endoscopic imaging systems allowing for low-UVA and UVA light transmissions. Schmidbauer *et al.* described the efficiency of flexible fluorescent cystoscopy in a study on 389 human bladder lesions. Fluorescent flexible cystoscopy had a 21% higher detection rate of CIS (82%) than standard flexible (61%) or standard rigid (67%) cystoscopy [21]. Wu and Qu found that the AF excited at 405 nm is sensitive to the cellular metabolism and can be used to sense the metabolic status of epithelial tissue [22].

The multiple scattering of photons carries information linked to morphological and structural characteristics of the tissue constituents. The shape and amplitude of the back-scattered intensity spectra are modified by the corresponding wavelength-dependent optical properties of absorption and diffusion. Statistical and empirical analysis of spectral features extracted from the DR spectra can be performed for finding out their correlations with some pathological states of the tissue. DR spectroscopy has already been applied to *in vivo* diagnosis in clinics, especially in cancerology for classifying healthy and pre-cancerous or cancerous tissues on oesophagus, breast, bladder and skin [13], [23]–[25]. Main DR spectroscopy studies on human bladder carcinomas indicate that very high sensitivity and specificity values may be obtained by exploiting the DR spectra slopes in the UVA region (between 330 and 370 nm) [26]. Much lower values are reported when considering only the visible wavelength band of the spectrum (400 to 700 nm) [27].

The interest in combining AF and DR spectroscopies to increase the efficiency of *in vivo* diagnosis (increased sensitivity and specificity) has been demonstrated in a number of clinical studies on cervix, oral cavity, breast and skin [12], [18], [28], [29]. For instance, spatially colocalized AF and DR measurements can be exploited to correct the measured AF spectra from absorption and diffusion by using the information brought by DR data. Various modeling approaches are currently developed to compensate these distortions and extract intrinsic fluorescence spectra of the tissue [30], [31]. These colocalized bi-modalities (AF and DR) measurements may also allow us to extract further spectral characteristics for selecting the most discriminant data combination with reference to the classification problem of the tissue under investigation. In the present study, we are interested in how improving the efficiency of *in vivo* bladder cancer discrimination when restraining the analysis to the NUV-Visible wavelength bandwidth. Therefore, we propose to combine AF excitation at 410 nm and DR excitation in the wavelength range 400-700 nm. Finally, the analysis of the spectral characteristics of the corresponding spectra and of the spatially resolved measurements requires three main steps of feature extraction, selection and classification successively.

The application of methods of *in vivo* optical spectroscopy implies to exploit some amplitude and shape features of the intensity spectra collected at various probing points on the tissue, so as to identify, non invasively, some pathological status of the tissue. The objective is usually to determine the belonging of the latter to a specific diagnostic category defined with reference to the gold standard histological expertise.

In spatially resolved bimodal spectroscopy, the measurement

data set collected on one point of the tissue consists in n_1 intensity spectra measured at n_2 inter-fiber distances (CEFS). These $n_1 \times n_2$ spectra acquired at n points on the tissue form a raw data matrix X of independent variables containing the numerical values of intensities observed for the p quantitative variables (with hundreds wavelengths per spectra). In the same time, the histopathological analysis of the n tissue samples (called individuals in the rest of the present paper) provides the reference values of class belonging. These discrete values form a class label vector Y (constituting the qualitative dependant variables). Consequently, the complexity of the data processing comes from very large size of the raw data matrix (thousands of variables p) compared to the small number of samples n intrinsically limited by the experiment potential. A rigorous selection of relevant data (significant or explicative variables) is needed to reduce the size of the spectral data set and to improve the performance and robustness of the models.

The present study aims at evaluating the efficiency of coupling AF and DR spectroscopies for bladder cancer diagnosis using excitations in a limited NUV-Visible wavelength range. The evaluation consists in finding the best diagnostic accuracy, i.e. the optimum [sensitivity, specificity] couple. This paper describes a bimodal instrumentation developed and applied in the frame of an experimental protocol performed on a pre-clinical model of cancer in rat bladder. Then, we present a detailed step-by-step analysis for the extraction and the selection of spectral features, and for the spectroscopic data final supervised classification.

II. MATERIALS AND METHODS

A. Instrumentation development and calibration

1) Description of the system: A spatially resolved bimodal optical spectroscopy instrumentation was developed for acquiring colocalized mono-excited autofluorescence (AF) and diffuse reflectance (DR) intensity spectra on biological tissues *in vivo* (Fig. 1). The Continuous-Wave bimodal light source consists of a laser diode source ($\lambda_{exc} = 410 \pm 5$ nm, Laser 2000, France) for AF excitation and a Deuterium-Tungsten Halogen light source (DH2000, Ocean Optics, France) for DR measurements in the wavelength range from 440 to 800 nm. Spatial resolution was obtained through the use of a multiple fiber probe whose distal tip was put in gentle contact with the surface of the tissue (rat bladder inner wall). Our probe contains 37-optical fibers (Si/Si fibers with 200 μm-core diameter and 0.22 numerical aperture, SEDI, France) arranged in concentric circles within the 2 mm diameter probe end. One fiber was chosen at the tip probe border for excitation and 13 other fibers were chosen for collecting backscattered light at different CEFS with the following center-to-center distances: 271, 340, 528, 599, 785, 834, 1002, 1036, 1076, 1187, 1296, 1442 and 1542 μm (Fig. 1). Indeed, this maximum number of 13 CEFS is due to a technical constraint of the multichannel imaging spectrograph (iHR 320, Horiba Jobin Yvon, France) whose entrance slit-to-fiber bundle adapter is limited to thirteen fibers in line, i.e. the simultaneous acquisition of 13 spectra. The latter spectrograph is based on a Czerny-Turner
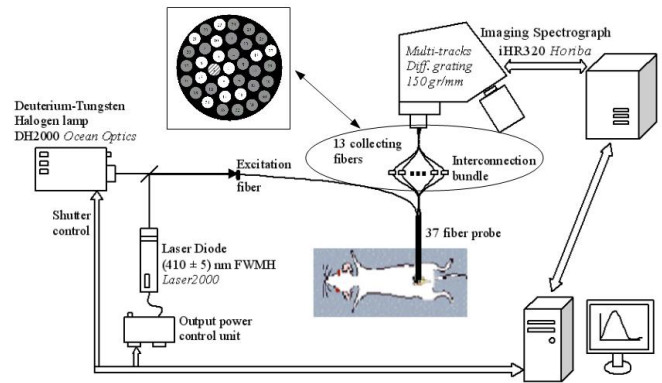

Fig. 1. Schematic representation of the bimodal spectroscopy device with a zoom on the multiple fiber probe (hatched gray fiber corresponds to the excitation fiber and white fibers to the emission fibers).

configuration (320 mm focal length) and equipped with a UV back-illuminated Charge Coupled Device detector (CCD-2048x512-BIUVSTE, Thermoelectric cooling (-70°C) E2V UV-treated Back Illuminated detector, Symphony controller, Horiba JY, France) and an emission filter-wheel with various filters used to reject the backscattered excitation light. Integration times were 2000 ms and 50 ms, respectively for AF and DR measurements. Spectra were all acquired using a diffraction grating with 150 gr/mm (blaze wavelength: 500 nm).

2) Calibration and Normalization procedures: The light intensity calibration required a light power adjustment using a power meter (841PE, power sensor UV 818-UV, Newport). To account for the wavelength dependence of the light source as well as for the fiber transmission and spectrometer spectral responses, a reference measurement of reflectance was regularly performed on a spectrally flat reflectance standard (Spectralon, WS-1 Diffuse Reflectance Standard, Ocean Optics, France) [13]. DR spectra were obtained by dividing each backscattered light intensity spectrum acquired on tissue by the backscattered light intensity spectrum obtained on this Lambertian surface diffusion standard. In order to improve signal to noise ratio, three acquisitions in a row were performed for each AF or DR spectrum before being averaged. All experimental spectra were pre-processed to correct the spectral distortions (wavelength and intensity) induced by the instrumentation. In order to improve reproducibility, a tripod was used for maintaining the tip of the optical fiber bundle in gentle contact to the bladder surface and perpendicular to it.

Optical resolution of the acquisition system was 2 nm. The calibration procedure was reiterated for each new biological tissue sample.

B. Biological materials and experimental protocol

1) Tumor cell culture and in vivo bladder instillation: Carcinomas were induced in rat bladder with cultured tumor cells from line AY-27. The rat bladder transitional cell carcinoma cell line AY-27 was established as a primary bladder

tumor in Fisher F344 rats by feeding FANFT (N-[4-(5-Nitro-2-furyl)-2-thiazolyl]- formamide), and was generously provided by Drs S. Selman and J. Hampton from the Medical College of Ohio (Toledo, OH). The culture medium used was RPMI-1640 (Gibco, Invitrogen, UK), supplemented with 5% L-glutamine, 5% penicillin-streptomycin and 10% fetal bovine serum (Biotech, GmbH). Cells were passaged when nearly confluent by standard, limited trypsinization procedures [32].

Tumor cell suspensions were prepared by mincing the tumor under sterile conditions and plating in sterile plastic T-175 flasks (175 cm^2) with 0.2 μm vented cap (BD Biosciences) and maintained in a humidified incubator with 5% CO_2 environment. When the cultured cells neared confluence, the medium was removed, and the cells were dissociated with 2 mL trypsin-EDTA for 10 min at $37°C$, then centrifuged, and re-suspended in complemented RPMI-1640 medium. Cells viability was determined by standard trypan blue (0.4%) exclusion test. Cells suspension directly from cell culture was used for bladder instillation. For orthotopic implantation, 4.10^6 cells in 1 mL were instilled intravesically [32].

42 female Fisher (F344) rats, weighing 115-150 g, were used for the experimental protocol (Harlan Laboratories, France). All animal procedures were performed according to institutional and national guidelines. Rodents were maintained in our animal care facility and housed four per cage at room temperature ($22°C \pm 2°C$) with food and water *ad libidum.*

Three groups of 14 rats each were established, with reference to three different incubation durations between the tumor cell administration day and the spectroscopic measurements day i.e. at 3, 7 and 14 days after tumor cell implantation. In each group, 10 rats were instilled with tumor cells, 3 rats were instilled only with HCl/NaOH and PBS and one healthy rat served as negative reference.

For tumor instillation, rats were anesthetized with an intraperitoneal injection of 45 mg.kg^{-1} sodium pentobarbital (Sanofi, France) and body temperature was maintained during experiments thanks to a thermostatic blanket. The rat bladder was catheterized with 16G intravenous cannula (Terumo, Surflo). Bladder epithelial desquamation was obtained through an intravesical instillation of 0.5 mL of HCl (0.1N) during 15 s, and neutralized with 0.5 mL of NaOH (0.1N) solution for 15 s, followed by PBS rinsing. Finally, a bladder tumor cell suspension was instilled intravesically for one hour. Sterile technique was used for tumor cells implantation. Finally, the catheter was removed and the rats were returned to their cage as soon as they were awoken.

2) Surgical protocol, spectroscopic measurements and histology: Spectroscopic measurements inside bladders were carried out on living rats. Each animal was anesthetized with pentobarbital at 45 mg.kg^{-1} (Sanofi, France) and a laparotomy was performed in order to access the bladder. The latter was incised for inserting the fiber optic probe end and performing spectroscopic measurements at distinct anatomical sites inside the bladder.

Intensity spectra were acquired on three different spots near urethra and ureters of each bladder. These places were marked with different colors of indelible Indian ink (blue, green, and black). Three spectra were acquired on each site in order to avoid any handling error and to collect enough data without having to include a larger number of animals to be sacrificed. Each animal was euthanized just after measurements and the bladder was excised for histological analysis and classification. Excised bladders were fixed in formaldehyde(CH_2O) solution before imbedding in paraffin. Tissue samples were serially sliced (5 μm thickness) with a microtome (Microm Heidelberg HM350, Germany), and stained with standard HE staining (Hematoxylin-Eosin) for histological examination. Histological slice images were realized with an optical transmission microscope (Olympus AX70, France).

C. Spectroscopic data preprocessing and feature extraction

At each anatomical point of measurement, three intensity spectra (in both AF and DR modalities) were systematically acquired then averaged in order to improve the signal to noise ratio. Residual high frequency noise was removed using a polynomial smooth filtering (Savitzky-Golay) applied overall each spectral curve between 440 and 800 nm. The window size and order of the filter were determined for each type of spectra (AF or DR) with reference to their specific shape characteristics. A 15 nm width window (2nd order) was applied to all AF spectra and 10 to 20 nm width windows (2nd order) were used for DR spectra. All spectra were analyzed (statistical tests, correlation with histological slides) in order to define, with greater precision, typical spectral features of normal and cancerous tissues, and to determine optimal measurement distances between excitation and illumination fibers.

Based on previous works by Mourant *et al.* [26], Koenig *et al.* [20], De Veld *et al.* [33] and on our own observations performed on the intensity peaks of interest and on the shapes of the spectral curves in specific bandwidths of wavelengths, we came to define a number of parameters with the following notation convention:

- P_{λ_i} stands for intensity Peak at λ_i,
- $A_{\lambda_i - \lambda_j}$ for Areas under the curve between λ_i and λ_j,
- $R_{P,A/A,P}$ for Ratios between intensity peaks and/or areas,
- $S_{\lambda_i - \lambda_j}$ for curve Slopes between λ_i and λ_j.

From AF and DR spectra, we calculated a first order approximation of intrinsic autofluorescence spectra (i.e. corrected from haemoglobin absorption) based on the approach of De Veld *et al.* [31] [33]. As stated by the equation below, it consists in dividing the AF spectra by the DR one (recorded at the same location) to some power to be determined.

$$F_i(\lambda) = \frac{F_a(\lambda)}{\exp(-\mu_a(\lambda)l_f)} = \frac{F_a(\lambda)}{R_d(\lambda)^{k_f(\lambda)}} \quad (1)$$

with $F_i(\lambda)$ the Intrinsic Fluorescence (IF) emission spectra of endogenous fluorophores, $F_a(\lambda)$ the bulk autofluorescence spectrum (measured), μ_a the absorption coefficient, l_f the mean free-path of autofluorescence in tissue, $R_d(\lambda)$ the diffuse reflectance spectra and k_f the ratio between the pathlengths for AF and DR light. The numerical value of this proportionality

parameter was obtained through a fitting procedure implementing a second order optimization procedure (non-linear least-squares Levenberg-Marquardt algorithm) and aiming at minimizing the area of a triangle formed by the F_i points at wavelengths 563, 582 and 604 nm (around the second blood absorption dip at 575 nm).

III. RESULTS AND DISCUSSION

A. Histological results and classification

We observed that tumor sizes obtained were not directly proportional to the delay following tumor cell implantation i.e. the instillation group. Variations were found in tumor size, degree of malignity and epithelium desquamation within and between groups. Actually, tumor growth is inevitably modulated by the tumor implantation location in the bladder and the proximity to blood vessels. The global conditioning and a global instillation lead to 100% tumors but randomly located. Due to practical constraints, it was not possible to have the histological classification available for each of the 126 excised samples (14 animals x 3 groups x 3 sites) at all steps of our spectral data classification algorithm described in the next sections. Thus, two complementary histological analysis were successively performed first on 98 excised samples then on the 28 remaining samples added to the 98 ones. Therefore, both histological analysis allowed us to classify the corresponding two data sets (98 then 126 sites) into three main classes of healthy (71 then 94 sites), inflammatory (9 then 9 sites), and tumoral tissue states (18 then 23 sites).

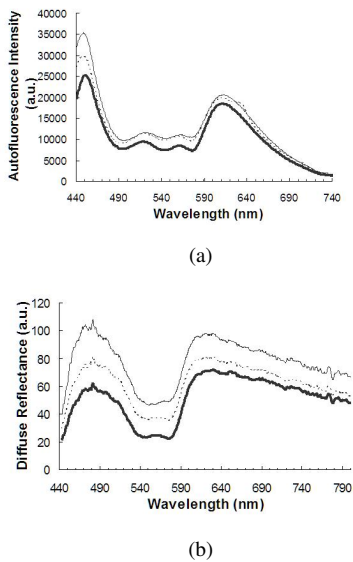### B. Spectroscopic results and spectral feature extraction

(a)

(b)

Fig. 2. Examples of 2(a) AF and 2(b) DR spectra measured at the shortest CEFS (271 μm) for tumoral (grey line), inflammatory (dotted line) and healthy (solid black line) tissue sites.

1) Autofluorescence results: Figure 2(a) gives an example of the pre-processed (spectrally corrected, smooth filtered) AF intensity spectra for healthy, inflammatory and tumoral tissues measured at the shortest CEFS (271 μm). For sake of figure clarity, spectra measured at other CEFS are not displayed but similar observations are noticed for all 13 other CEFS. We may observe a rather remarkable shape for the autofluorescence spectra whose amplitude is modulated by haemoglobin absorption between 490 and 690 nm (for example, peak at 565 nm, hollows at 540 and 575 nm). Furthermore, the overall amplitude of the AF intensity spectra vary as a function of the tissue status considered with higher amplitude for tumoral tissues and lower amplitude for healthy ones. In our case, the results obtained are opposite to those referenced on human bladder tissue *in vivo* for which tumoral tissues generally produce a lower level of autofluorescence intensity than healthy ones [34]. This may be due to the nature of our experimental model used and more exactly to the experimental procedure which implies surgery and consequently bleeding at the inner surface where measurements are performed. In our laboratory, previous work on the same animal model of bladder tumor rat have shown similar results [35].

Looking more precisely at curves on Fig. 2(a), it can be noticed a fluorescence decrease attributed to the haemoglobin absorption in the 525-575 nm range. When we observe the hollows at 540 and 575 nm corresponding to the absorption peaks of oxyhaemoglobin HbO_2, we may notice that the bumps in the spectral curves of tumoral tissues between 490 and 590 nm have a lower amplitude than those of healthy tissues. This result may also be explained by the nature of the tumoral model used and the thickness of the bladder wall. The mean wall thickness of a normal bladder in the conditions of experimentation (after filling with physiological water) is 100 to 300 μm. This thickness is of the order of about 500 to 800 μm for a two-weeks tumor. Indeed, in the case of healthy bladders, much of the incident light is scattered and transmitted throughout the wall, whereas a larger amount of light is scattered and absorbed in thicker tumor tissues thus generating an increased level of resulting AF intensity.

To statistically verify the observation made that the spectrum bump's amplitudes at 520 and 565 nm are lower for the tumoral tissues than for healthy ones, we calculated the ratio between autofluorescence intensities at 615 and 520 nm $R_{P_{615}/P_{520}}$ and the ratio between the autofluorescence intensities at 615 and 565 nm $R_{P_{615}/P_{565}}$. Statistically significant differences were noted between healthy and tumoral tissues.

2) Diffuse reflectance results: Figure 2(b) represents an example of the diffuse reflectance spectra for tumoral, inflammatory and healthy tissues acquired at the shortest CEFS (271 μm).

The overall shapes of these spectra appear identical whatever the tissue considered. The diffuse reflectance intensity is generally weaker for healthy samples than for inflammatory ones, and the latter also weaker than tumoral tissues. We also noticed that the absorption peaks in DR curves are less pronounced in tumoral than in healthy tissue samples.

From the observations made on these DR spectra, we propose to calculate further simple spectral indices of potential interest

for differentiating between the three histological classes of interest. The notation convention applied is the one already mentioned in section II-C. The subscript will denote the wavelengths concerned with the measure, and the superscript indicates the number of the measurement fiber involved. With these conventions in mind, our extracted variables were (with the fiber's number nf $\in \{1..13\}$):

- $A_{440-560}^{\text{nf}}$ and $A_{440-800}^{\text{nf}}$ respectively the partial area under the curve between 440 and 560 nm and the total area under the curve between 440 and 800 nm, at every CEFS,
- $R_{P_{480}/A_{440-800}}^{\text{nf}}$ the ratio between the peak value at 480 nm and area under the curve,
- $R_{P_{740}/A_{440-800}}^{\text{nf}}$ the ratio between the peak value at 740 nm (haemoglobin hollow) and area under the curve,
- $S_{440-470}^{\text{nf}}$, $S_{590-615}^{\text{nf}}$ and $S_{650-750}^{\text{nf}}$ the slopes calculated on DR spectra respectively between 440 and 470 nm, between 590 and 615 nm and between 650 and 750 nm.

The slopes calculated between 440 and 470 nm appear to be the most representative feature for the tissues considered (Fig. 3) confirming what was initially shown by Mourant *et al.* [26] on human bladders. In the present study, a slope value below 2.5 a.u./nm corresponds to healthy tissues while a higher value is related to tumoral ones.
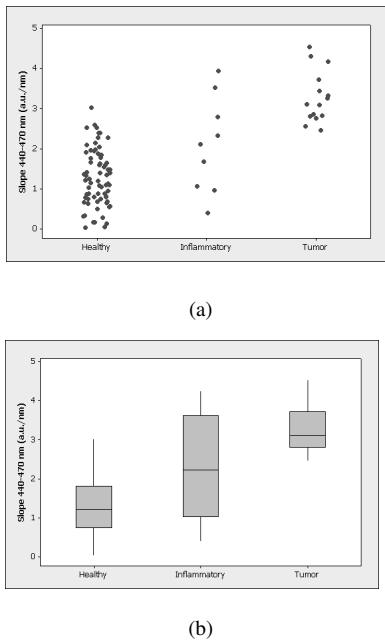

(a)

(b)

Fig. 3. 3(a) Slope values between 440-470 nm for tissue samples of all histological classes, 3(b) Box and Whiskers Plots also representing slopes.

The visual observation of the histological slides did not allow us to distinguish precisely between intermediate stages of the inflammatory tissues: most of the inflammatory sites correspond to the rat group for which measures were conducted three days after instillation. Thus, the bladder epithelium did not have enough time to "heal", hence the difficulty of histological finest expertise.

3) Intrinsic Fluorescence: Figure 4 represents intrinsic fluorescence mean spectra at the shortest CEFS (271 μm)

for healthy, inflammatory and tumoral rat bladder tissues and their corresponding optimized mean values of $k_f \pm SD$. These spectra are normalized with reference to the maximum peak value of the healthy tissue spectra.
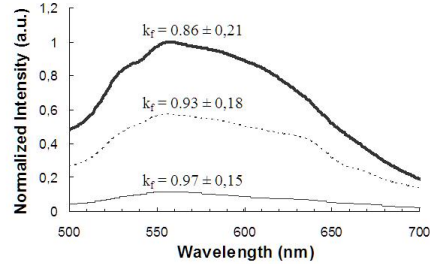

Fig. 4. Intrinsic fluorescence mean spectra and corresponding mean values $\pm SD$ of k_f for healthy (solid black line), inflammatory (dotted line) and tumoral tissues (grey line).

By this way of minimizing the influence of blood absorption on raw AF spectra, a difference can be seen when comparing the intrinsic fluorescence spectra (Fig. 4) and non-normalized autofluorescence spectra (Fig. 2(a)). Moreover, the residual peaks are more pronounced on healthy tissues (solid black line) than on tumoral tissues (grey line), because of a higher influence of haemoglobin. The intensity level of intrinsic fluorescence is lower for tumoral tissue than for inflammatory tissue, which is lower than for healthy tissues. This is probably associated with a weaker concentration of fluorophores and/or the presence of a thickened surface layer, possibly more absorbing. These results are consistent with *in vivo* measurements on patients because the relative amplitude of the intrinsic fluorescence spectra of our model are therefore well correlated with the ones of the autofluorescence spectra of the human bladder [34].

We then calculated and compared different parameters by means of statistical tests: coefficient k_f, maximum values of peaks (wavelength and amplitude) and areas under curve between 500 and 700 nm. As noted previously, we have statistically significant differences between healthy and tumoral tissues, between inflammatory and tumoral tissues, and between healthy and inflammatory tissues. We can put forward that the increasing values of k_f with inflammation and tumor is coherent with a corresponding thickening of the bladder wall. At the inter-fiber distance of 271 μm, the mean value of k_f is 0.86 for healthy tissues and 0.97 for tumoral tissues, which indicates that the fluorescence photons seem to travel a relatively longer path in tumor tissues.

C. Spectral feature statistical analysis, selection and classification

This section is devoted to the statistical analysis of the spectral data extracted as described above, and we shall first say a few words about the way statistics enter into the study for other articles dealing with cancer detection by spectral methods. Most of them [12], [16], [17], [25], [28], use first Principal Component Analysis (PCA) in order

to reduce the huge dimension of each data. Then, with the principal components in hand, a Logistic Regression Analysis (LRA) is applied in order to separate classes in [12], [16], [17] while univariate tests (Wilcoxon test to be specific) were used in [25] in order to discriminate variables and [28] relies on PCA-based classification. While these procedures are perfectly reasonable, they all raise at least two problems from a statistical point of view: (i) PCA might not be the optimal dimension reduction technique in this context, and Linear Discriminant Analysis (LDA) methods are arguably better fitted for dimension reduction when one has a variable selection procedure in mind. Moreover, PCA produces intricate combinations of variables, which are hard to interpret *a posteriori* from a biological point of view. (ii) No real multivariate variable selection techniques are considered in the aforementioned references, and one goes directly from PCA dimension reduction to classification methods, mainly based on logistic regression. Based on these considerations, we shall try to see if a sharper statistical treatment of our data can lead to a better classification of the tissues at hand.

Our aim here is thus twofold: we shall first select a reasonable number of discriminating variables among the characters extracted from the AF, DR and IF spectra. This step will only rely on classical classification methods such as LDA or LRA (as in the references quoted above), which are arguably robust enough for variable selections. At the end of this procedure, we will be able to identify 16 discriminating variables. Then, in a second step of the study, we shall use some sharper classification techniques (Regularized Discriminant Analysis RDA and Support Vector Machines SVM to be specific) in order to get an accurate classification boundary between cancer and healthy tissues, on the basis of our 16 selected variables. In the end, a Leave-One-Out (LOO) scheme using SVMs with a Gaussian kernel will lead to a sensitivity of 87% and a specificity of 77%.

It should also be mentioned at this point that all our computational procedures were performed by means of the R program. We will specify in some cases the exact R function which was used.

1) Presentation of the data for the supervised classification: According to Section II-C, the data we have to handle can be described as follows: on a set of tissue samples or individuals $I = \{1, \ldots, n\}$, we measured p quantitative variables $x^1, \ldots, x^p$, where n represents the number of bladder sites under consideration, and where p stands for the number of area, peak, ratio and slope variables measured on the spectra. More specifically, 8 variables were pre-selected for the AF spectra, 6 for the DR spectra, and 2 for the IF spectra, so that 16 variables are considered for each CEFS. Taking into account that we have 13 collecting fibers at our disposal, we end up with $p_1 = 208$ characters for each individual at the beginning of the study.

Let us say a word about the number n of individuals: as mentioned in Section III-B, a simple Mann-Whitney test reveals that it is hard to distinguish inflammatory from cancer tissues on the basis of the variables we are considering.

This impression is also easily confirmed by a plot of the data with dimension reduction (not included here for sake of conciseness). We have thus decided, for the variable selection procedure, to separate the inflammatory tissues from the other ones. This means that only the 71 healthy and 18 tumoral tissues are considered for the first step of our study, and hence $n = 89$. In particular, notice that $p \gg n$, so that a dimension reduction is certainly necessary.

Our experience also includes the measurement, on each individual, of a qualitative character y taking values in $\{1, 2\}$, where 1 indicates that the tissue is considered as healthy and 2 that it is cancerous. These values define a partition I_1, I_2 of the set I. In this context, the two steps of our study can be summarized as: *(i)* Select a small number of variables out of $x^1, \ldots, x^p$, still allowing a good separation between I_1 and I_2 *(ii)* Find the best possible relation between y and the selected variables according to the available data.

Here are some additional notations for our study: for $k = 1, 2$, we set $n_k = |I_k|$ the cardinality of a finite set I_k. Recall that for the first step of our analysis, we have $n_1 = 71$ and $n_2 = 18$. For $k = 1, 2$, $i \leq n_k$, $j \leq p$, we also set x_{ki}^j for the value of the jth character for the ith individual of the kth class. The total covariance matrix T will also appear in the sequel. Considering each character vector x_{ki} in $\mathbb{R}^p$, and denoting by x_{ki}^* the transposed of this vector, it is defined by:

$$T = \frac{1}{n} \sum_{k=1,2} \sum_{i=1}^{n_k} (x_{ki} - m)(x_{ki} - m)^* \qquad (2)$$

where m stands for the mean of all our data.

2) Elimination of characters: As mentioned in Section III-C1, due to the small size of our individuals sample, it is necessary to reduce drastically the number of characters to consider for classification purposes. This dimension reduction will be performed in three steps: *(i)* We first analyze the discrimination power of each character individually, and keep only the most discriminating ones. *(ii)* It is also important to recall that 13 collecting fibers i.e. 13 different inter-fiber distances (CEFS) are involved in our experiment. Therefore, we expect to observe many correlated characters. We decided to group those very correlated characters, and to keep only the most discriminating one among each group. Notice that the first elementary steps (i) and (ii) allow to drop the number of characters from 208 to 51. *(iii)* Starting from those 51 characters, we performed some stepwise selection procedures, which allowed us to end up with 16 characters only.

We now proceed to detail the three steps alluded to above.

Testing equality of distributions

The first natural step for a good dimension reduction is to consider each character $x^1, \ldots, x^p$ individually, and to test its discrimination power between I_1 (healthy individuals) and I_2 (cancer individuals). Let us then $x \in \mathbb{R}$ be a character chosen among $x^1, \ldots, x^p$. The first idea a statistician may have in mind in order to test the discriminating power of x is to use the Student t-test. However, in order to select

variables with a t-test, it is important to verify that they can be assumed to be normally distributed. For small or medium sized samples like ours, the standard normality test is Shapiro-Wilk's one [36]; this test, performed on all the variables, asserts that most of our characters can not be considered as Gaussian. More specifically, taking class 2 as an example, we found 119 variables with a p-value lower than 0.02 for the Shapiro-Wilk test, and 133 with a p-value lower than 0.05.

We thus decided to select variables according to Mann-Whitney's test only, since this test does not depend on the particular shape of the underlying probability distribution and is well adapted to medium sized samples. By doing so, and keeping only the characters yielding a p-value lower than 0.02, we retained 26 variables for the AF spectra, 59 for the DR ones, and 7 for the IF ones, that is $p_2 = 92$ variables in total.

Correlation analysis

Another elementary step consists in grouping all the highly correlated characters, and choose only the best discriminating character among those groups. This step is important, since it permits to reduce dimension, avoid redundancy, and also prevents us from manipulating almost degenerate matrices in our future computations.

We thus go back to the total covariance matrix T given by (2), and define the correlation coefficient $\rho_{jj'}$ between characters j and j' as $\rho_{jj'} = T_{jj'}/\sigma_j\sigma_{j'}$, where $T_{jj'}$ is the covariance matrix between characters x^j and $x^{j'}$, and σ_j stands for the standard deviation of x^j. Then we gather all the pairs (j, j') of characters having a correlation coefficient $\rho_{jj'}$ satisfying $|\rho_{jj'}| \geq 0.95$. For those groups, we only select the character i_0 exhibiting the lowest p-value for the Mann-Whitney test performed above.

This simple correlation analysis allows for reducing the number of variables to 15 variables for the AF spectra, 29 for the DR ones, and 7 for the IF ones, that is $p_3 = 51$ variables in total.

Interestingly enough, we have not found any pair of characters (j, j') coming from different kind of spectra and exhibiting a correlation coefficient $\rho_{jj'}$ satisfying $|\rho_{jj'}| \geq 0.95$. This seems to indicate that the combination of the three methods of spectral analysis may lead to an improvement in our supervised classification.

Once the first selection steps of Sections III-C2 have been performed, it can be useful to settle a LDA representation, in order to verify that the $p_3 = 51$ variables we are dealing with can serve to separate our data accurately. Let us recall that LDA is a geometrical method which allows for reducing the data dimension, with a criterion ensuring the best possible separation between classes. As a preliminary study, it helps to visualize if our data have a chance to be sufficiently separated according to our labels y (see [37], [38] for a complete account on the topic).

Notice that for 2 classes, the discriminant analysis projection is necessarily one-dimensional, and the two projected distributions are visualized in Figure 5. The good separation exhibited on this picture can be corroborated numerically. Indeed, the
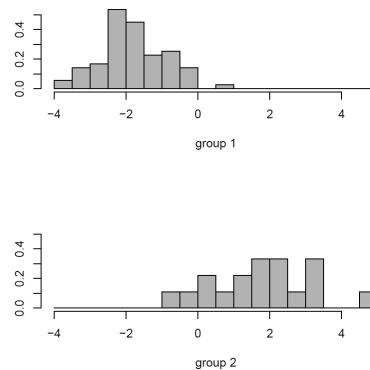

Fig. 5.   Discriminant analysis for the $p_3 = 51$ selected variables (vertical axis: normalized number of individuals; horizontal axis: group 1 = healthy, group 2 = tumoral).

discriminant analysis also induces the computation of a linear separation boundary (see [37], [38] again for further details), and thus a linear prediction function. This procedure, applied to our data, leads to a sensitivity of 77.8% and a specificity equal to 98.6%. These encouraging results seem to indicate that it is reasonable to go on with our study with the $p_3 = 51$ variables selected up to now.

Stepwise selection

The last step in our variable selection is to start from the $p_3 = 51$ variables selected above, and apply them a more systematical variable reduction treatment, called (forward or backward) stepwise selection. This method is an iterative scheme, allowing at each step to aggregate (in the forward case) or drop (in the backward case) a character according to its discriminating power in the presence of the other selected characters. The discriminating power is always measured through a statistical criterion, and we have chosen here to work with three criterions which are computationally adapted to our data, based respectively on LDA, analysis of variance (Wilk's test to be specific) and Logistic Regression models (LRA). In the end, the accuracy of the stepwise selection is measured by a confusion matrix assessing the proportion of well-classified individuals in each group.

It happens that the method (among those we have tested) which gives the best results in terms of confusion matrices is a backward selection based on logistic regression models. For sake of conciseness, we will thus only give an account on this specific procedure. Indeed, the backward selection based on logistic regression models is implemented in R through a function called glm. Running this function on our data, we obtain $p_4 = 16$ selected variables, with a confusion matrix given in table I hereafter.

In our context, it seems reasonable to work with $p_4 = 16$ variables for classification purposes, this number being consistent with the size of our sample. Since the logistic classifier performs better than the ones based on LDA or Wilks methods, we have chosen to keep all those p_4 variables for

TABLE I
CONFUSION MATRIX OBTAINED FROM BACKWARD SELECTION
PROCEDURE BASED ON LRA (LOGISTIC REGRESSION ANALYSIS) WITH
LINES/COLUMNS 1 AND 2 CORRESPONDING RESPECTIVELY TO HEALTHY
AND CANCEROUS TISSUE CLASSES.

Real\Predicted	1	2
1	70 (98.6%)	1 (1.4%)
2	6 (33.3%)	12 (66.7%)

the end of our study. For sake of completeness, our selected variables are (with the notation convention already mentioned in Section II-C):

AF: P_{520}^8, $A_{440-740}^8$, P_{520}^{13}.

DR: $A_{440-740}^1$, P_{560}^1, P_{740}^1, $R_{740-480}^1$, $A_{440-740}^2$, P_{740}^2, P_{480}^4, $S_{440-470}^4$, P_{480}^5, P_{480}^7, P_{560}^7, $S_{440-470}^7$, $S_{440-470}^8$.

It is worth mentioning at this point that most of the 13 fibers contribute to the selected variables, which means that a restriction to one fiber only would lead to a dramatic loss of information. We should also stress the following consistence between the selection methods we have chosen: indeed 7 characters, out of the 8 we have selected according to the LDA criterion, are also selected by the logistic procedure. However, the variables chosen according to Wilks' criterion are rather different, and we believe that it is due to the fact that the latter methods heavily rely on Gaussian assumptions for the variables involved in the study.

3) Classification: Our variable selection has been performed according to some reasonable classification criterions (recall that we have used LDA, Wilks' criterion and logistic regression). However, with the $p_4 = 16$ discriminant characters we have exhibited, one can try to improve our classification results, by resorting to some more sophisticated tools. We have implemented this strategy in the following way:

(i) We go back to our initial data (as referred in Section III-A), consisting in 126 sites, with a final global sample consisting in 94 healthy sites, 23 cancerous sites, and 9 inflammatory sites. The number of inflammatory sites being once again too small with respect to the other ones, we discard them from the remainder of the study, and we focus on the 94 healthy and 23 cancerous tissues. For the classification procedure, we thus consider a sample of size $n = 117$, with $n_1 = 94$ and $n_2 = 23$. We then try to construct an accurate boundary separating these samples. Notice that, due to the important rate of healthy tissues, it is expected that the sensitivity of our test will behave worse than its specificity.

(ii) Our classification scheme relies on two modern (yet already classical) methods, respectively RDA and SVM, allowing for constructing separation boundaries in a wide number of situations. We measured their performance on our data by a crossed-validation procedure of LOO type.

Let us describe now the results obtained through RDA type methods. Introduced by Friedman in [39], this technique allows to interpolate between LDA, quadratic discriminant analysis and geometric classification. For RDA classification,

the function which can be used in the software R is called `rda`, and this procedure also optimizes interpolation coefficients. It should be noticed however that, for our particular data, the RDA method seems to be quite inefficient. Indeed, the optimal coefficients found by the algorithm induce a classification method very close to LDA. And for those optimal coefficients, the LOO procedure yields a specificity of 94.41%, but a sensitivity equal to 17.39% only. These bad results shouldn't be too alarming though. They simply indicate that the accurate separation boundary between cancerous and healthy tissues is more complex than a linear or quadratic one.

This impression is confirmed by an analysis using SVMs. The support vector machines method, developed initially by Vapnik [40] and nicely introduced in [41], gives another way to construct a boundary separating our data $\{x_i; i \leq n\}$ in $\mathbb{R}^{p_4}$, according to the labels y_i. This boundary is given by a hyperplane maximizing the minimal distance between each class and any separating hyperplane. Furthermore, one of the great advantages of the method is that it can easily be generalized to some highly non linear situations, by means of some implicit change of variables given by kernels. For our data, we have resorted to a Gaussian kernel given by $K(x, y) = \exp(-\gamma\|x-y\|^2)$, that is one of the typical example of kernels used in non linear situations. Tuning the value of γ to $\gamma = 1.55$ (which seems to be a good balance between precision and over-fitting), we run the `svm` function on R on our set of data. The cross-validation procedure gave then the following confusion matrix (table II):

TABLE II
CONFUSION MATRIX OBTAINED FROM LOO (LEAVE-ONE-OUT)
CROSS-VALIDATION PROCEDURE BASED ON SVM (SUPPORT VECTOR
MACHINE) WITH LINES/COLUMNS 1 AND 2 CORRESPONDING
RESPECTIVELY TO HEALTHY AND CANCEROUS TISSUE CLASSES.

Real\Predicted	1	2
1	72 (76.6%)	22 (23.4%)
2	3 (13%)	20 (87%)

This result is, from our point of view, a good compromise between sensitivity and specificity. We can conclude that combining AF (410 nm-excitation), DR, and IF parameters gives superior results to AF alone, or DR alone. With the combination of two modalities, we obtain a lower sensitivity than Koenig *et al.* (respectively 77% vs 91%) and a higher specificity (87% vs 60%). Koenig *et al.* work in human bladder (26 bladders) with diffuse reflectance (400-700 nm) [27]. In elastic scattering, Mourant *et al.* [26] obtained a sensitivity equal to 100% and a specificity equal to 96% for detection of human bladder carcinoma (10 patients), based on the values of the slopes over the wavelength range 330-370 nm.

IV. CONCLUSION

A simple fibered spectroscopy instrumentation was developed to acquire both AutoFluorescence (AF) and Diffuse Reflectance (DR) spectra in a bimodal approach at several CEFS and applied *in vivo* to monitor healthy to cancerous evolution of rat bladders. Bimodal spectroscopy's accuracy

in discriminating three classes of bladder histological stages was evaluated: healthy, inflammatory and tumoral stages. Various sets of spectral characteristics (extracted from the spectral intensity curves) were selected based on statistical discrimination. At a technical level, the SVM method is known to be very flexible. It shows here to be really adapted to the data set we had to handle, for which the boundary seemed more intricate than a simple quadratic function. More interestingly, it is satisfying to see that the combination of AF and DR spectroscopies allows us to discriminate accurately between cancerous and non cancerous tissues, with a reasonable number of parameters (recall that we took $p_4 = 16$). In spite of the small size of our sample, we were able to reach a high sensitivity (87%) and a good specificity (77%) for a Leave-One-Out procedure. The method presented here exploits bimodal spectroscopic measures in the harmless (non mutagenic) near UV-Visible wavelength band, combined to a dedicated spectral data selection and classification scheme. Hence, significant differences between healthy, inflammatory and tumoral tissues were obtained from the combination of particular features from AF, DR and Intrinsic Fluorescence spectra, with improved sensitivity and specificity compared to monomodality (AF or DR alone). This method could be applied in clinics as a complementary decision-making help tool for non invasive *in vivo* cancer diagnosis.

Acknowledgment

References

[1] V. Backman *et al.*, "Detection of preinvasive cancer cells," *Nature*, vol. 406, pp. 35–36, 2000.
[2] M. Skala *et al.*, "Investigations of Fiber-Optic probe designs for Optical Spectroscopic Diagnosis of Epithelial Pre-Cancer," *Laser Surg. Med.*, vol. 34, pp. 25–38, 2004.
[3] J. Tyczynski and D. Parkin, "Bladder cancer in Europe," *ENCR Cancer Fact Sheets. International Agency for Research on Cancer*, vol. 3, September 2003.
[4] C. Lee, "Bladder Cancer." American Urological Association, San Antonio, Texas, 2005.
[5] B. Jacobs, C. Lee, and J. Montie, "Bladder Cancer in 2010, How far have we come ?" *CA Cancer J Clin*, vol. 60, no. 4, pp. 244–272, 2010.
[6] V. Lokeshwar and M.S.Soloway, "Current bladder tumor tests : does their projected utility fulfill clinical necessity ?" *J. Urology*, vol. 165, no. 4, pp. 1067–1077, 2001.
[7] S. Wilczynski, *Introduction to the Diagnostics of Cancer, The Cancer Handbook*. Nature Publishing Group, 2001, ch. 33, pp. 461–475.
[8] T. Vo-Dinh, *Biomedical Photonics Handbook*. CRC Press, 2003.
[9] B. Young, A. Stevens, and J. Lowe, *Wheater's Basic Histopathology: A Colour Atlas and Text*, 4th ed. Churchill Livingstone, 2002.
[10] A. Shmilovici, "Incomplete tumor volume reduction may improve cancer prognosis," *Medical Hypotheses*, vol. 68, pp. 1236–1239, 2007.
[11] J. Quincy Brown *et al.*, "Quantitative optical spectroscopy: a robust tool for direct measurement of breast cancer vascular oxygenation and total hemoglobin content in vivo," *Cancer Res*, vol. 69, pp. 2919–2926, 2009.
[12] I. Georgakoudi *et al.*, "Fluorescence, reflectance, and light-scattering spectroscopy for evaluating dysplasia in patients with Barrett's Esophagus," *Gastroenterology*, vol. 120, pp. 1620–1629, 2001.
[13] O. A'Amar and I. Bigio, "Spectroscopy for the Assessment of Melanomas," in *Reviews in Fluorescence 2006*, vol. 3. Springer, New York, 2006, pp. 359–386.
[14] R. Drezek *et al.*, "Understanding the contributions of NADH and collagen to cervical tissue fluorescence spectra: Modeling, measurements, and implications," *J. Biomed. Opt.*, vol. 6, no. 4, pp. 385–396, 2001.
[15] E. Drakaki *et al.*, "*In vitro* fluorescence measurements and Monte Carlo simulation of laser irradiation propagation in porcine skin tissue," *Lasers Med. Sci.*, vol. 23, pp. 267–276, 2008.
[16] I. Georgakoudi *et al.*, "Tri-modal spectroscopy for the detection and characterization of cervical precancers *in vivo*," *Am. J. Obstet. Gynecol.*, vol. 186, no. 3, pp. 374–382, 2002.
[17] N. Ramanujam *et al.*, "Development of a Multivariate Statistical Algorithm to Analyze Human Cervical Tissue Fluorescence Spectra Acquired In Vivo," *Laser Surg. Med.*, vol. 19, pp. 46–62, 1996.
[18] H. Zeng *et al.*, "Spectroscopic and microscopic characteristics of human skin autofluorescence emission," *Photochem. Photobiol.*, vol. 61, no. 6, pp. 639–645, 1995.
[19] W. Zheng *et al.*, "Optimal excitation-emission wavelengths for autofluorescence diagnosis of bladder tumors," *Int. J. Cancer*, vol. 104, pp. 477–481, 2003.
[20] F. Koenig *et al.*, "Autofluorescence guided biopsy for the early diagnosis of bladder carcinoma," *J. Urology*, vol. 159, pp. 1871–1875, 1998.
[21] J. Schmidbauer *et al.*, "Flexible hexyl-aminolevulinate fluorescence cystoscopy in detecting high risk bladder cancer." Abstract 855, American Urological Association, San Antonio, Texas, 2005.
[22] Y. Wu and J. Qu, "Combined depth- and time-resolved autofluorescence spectroscopy of epithelial tissue," *Optics Letters*, vol. 31, no. 12, pp. 1833–1835, 2006.
[23] R. Gurjar *et al.*, "Imaging human epithelial properties with polarized light scattering spectroscopy," *Nat. Med.*, vol. 7, pp. 1245–1248, 2001.
[24] Y. Mirabal *et al.*, "Reflectance spectroscopy for in vivo detection of cervical precancer," *J. Biomed. Opt.*, vol. 7, no. 4, pp. 587–594, 2002.
[25] C. Zhu *et al.*, "Diagnosis of breast cancer using diffuse reflectance spectroscopy : Comparison of a Monte Carlo versus partial least squares analysis based feature extraction technique," *Laser Surg. Med.*, vol. 38, pp. 714–724, 2006.
[26] J. Mourant *et al.*, "Spectroscopic diagnosis of bladder cancer with elastic light scattering," *Laser Surg. Med.*, vol. 17, no. 4, pp. 350–357, 1995.
[27] F. Koenig *et al.*, "Spectroscopic measurement of diffuse reflectance for enhanced detection of bladder carcinoma," *Urology*, vol. 51, no. 2, pp. 342–345, 1998.
[28] S. Chang *et al.*, "Combined reflectance and fluorescence spectroscopy for *in vivo* detection of cervical pre-cancer," *J. Biomed. Opt.*, vol. 10, no. 2, pp. 1–11, 2005.
[29] G. Palmer *et al.*, "Comparison of Multiexcitation Fluorescence and Diffuse Reflectance Spectroscopy for the Diagnosis of Breast Cancer," *IEEE Trans. Biomed. Eng.*, vol. 50, no. 11, pp. 1233–1242, 2003.
[30] K. Badizadegan *et al.*, "Spectroscopic diagnosis and imaging of invisible pre-cancer," *Faraday Discuss.*, vol. 126, pp. 265–279, 2004.
[31] D. De Veld *et al.*, "The status of *in vivo* autofluorescence spectroscopy and imaging for oral oncology: Review," *Oral Oncol.*, vol. 41, no. 2, pp. 117–31, 2005.
[32] S. El Khatib *et al.*, "A novel orthotopic bladder tumor model with predictable localization of a solitary tumor," *Cancer Biol Ther.*, vol. 5, no. 10, pp. 1327–1331, 2006.
[33] D. De Veld, "Autofluorescence spectroscopy for the classification of oral lesions," Ph.D. dissertation, University of Groningen, 2005.
[34] M. Anidjar *et al.*, "The role of laser-induced autofluorescence spectroscopy in bladder tumor detection: dependance on the excitation wavelength," *Annals New York Academy of Sciences*, pp. 130–142, 1998.
[35] J. Padilla Ybarra, "Biopsie optique par spectroscopie de fluorescence des tissus vivants," Ph.D. dissertation, INPL, 1999.
[36] S. Shapiro and M. Wilk, "An analysis of variance test for normality: Complete samples," *Biometrika*, vol. 52, pp. 591–611, 1965.
[37] L. Lebart, A. Morineau, and K. Warwick, *Multivariate descriptive statistical analysis*, 3rd ed. John Wiley and Sons, 1984.
[38] G. Mc Lachlan, *Discriminant analysis and statistical pattern recognition*, 3rd ed. John Wiley and Sons, 1992.
[39] J. Friedman, "Regularized discriminant analysis," *J. Amer. Statist. Assoc.*, vol. 84, no. 405, pp. 165–175, 1989.
[40] V. Vapnik, *Statistical learning theory*. John Wiley and Sons, 1998.
[41] N. Cristianini and J. Shawe-Taylor, *An introduction to Support Vector Machines and other kernel-based learning methods*. Cambridge University Press, 2000.